Principal stress orientations of the Nankai Trough megathrust constrained by seismic and aseismic slip

Tyler Newton and Amanda Thomas
University of Oregon, Department of Earth Sciences, Eugene, OR, USA
tnewton@uoregon.edu

ABSTRACT

The strength of subduction thrust faults, or megathrusts, is key to understanding seismogenesis at the provenance of Earth's largest earthquakes. Earthquake focal mechanisms are routinely inverted to constrain the stress state at seismogenic depths. The stress state of megathrusts is expressed not only by earthquakes, but also by types of slow fault slip that are measured geodetically. Previous studies conducting earthquake-only stress inversions have found principal stress orientations in the Nankai Trough region of Japan that are incompatible with the tectonic setting. We introduce focal mechanisms of short term slow slip events (SSEs), a type of slow fault slip, in conjunction with earthquake focal mechanisms into a regional stress inversion to investigate the stress state of the Nankai Trough megathrust and interpret the results in the context of the regional tectonics. When SSEs are considered, the stress state of the central and eastern Nankai Trough megathrust is well-oriented for thrust faulting. Our results suggest that areas hosting SSEs and other slow fault slip may appear to have misoriented stress fields if slow fault slip constitutes a substantial proportion of fault slip and is not included in the stress analysis. The stress field in different tectonic regimes provides insight into the mechanics of faulting for the considered region, so stress analyses that include SSEs may help illuminate the temporal evolution of controls on fault stress, like pore pressure.

MOTIVATION

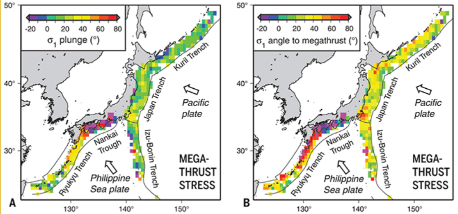

Figure 1. From Hardebeck (2015), a previous study that revealed stress orientations that are misoriented for megathrust faulting in the Nankai Trough region of Japan, which spatially coincides with slow slip events (SSEs). 1A shows the plunge of the maximum compressive stress axis, σ_1, relative to the surface. 1B shows the spatial distribution of the angle of σ_1 to the megathrust interface.

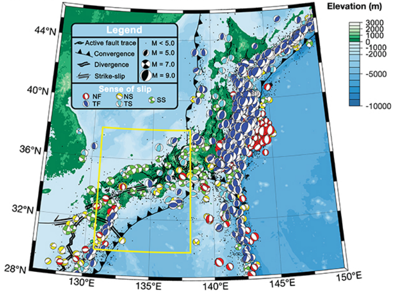

Figure 2. Regional seismicity of Japan. Yellow box denotes the study area. Locations of earthquakes considered in this study are denoted by black dots and focal mechanisms of size and color corresponding to magnitude and sense of slip, respectively. NF, TF, NS, TS, and SS denote normal faulting, thrust faulting, oblique normal faulting with a strike-slip component, oblique thrust faulting with a strike-slip component, and strike-slip faulting, respectively.

DATA & METHODS

DATA SOURCES

1. Earthquakes, 1229 events:
   NIED Seismic Moment Tensor Catalog from 1997-2015 (Okada et al., 2004)
2. SSEs, 368 events:

Source	# of events
Sekine et al. (2010)	48
Nishimura et al. (2013)	140
Nishimura (2014)	222
Kano et al. (2018)*	120

*Data obtained from the Science of Slow Earthquakes database. Dataset includes the work of Itaba and Ando (2011); Kitagawa et al. (2011); Itaba et al. (2012); Kitagawa et al. (2012); Itabaet al. (2013a, 2013b, 2014a, 2014b); Ochi et al. (2015, 2016). SSE data spans 1997-2015.

METHODS

1. ETAS declustering with SEDA (Lombardi, 2017)
2. k-means++ spatial clustering of events (Arthur & Vassilvitskii, 2007)
3. Damped least-squares stress inversion with MSATSI (Martinez-Garzon et al., 2014) incorporating fault instability analysis (Vavrycuk, 2014) to identify nodal planes and estimate coefficient of friction.

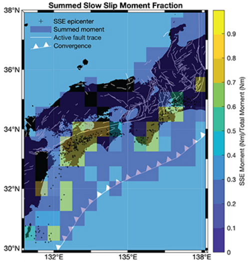

Figure 3 (above). The fraction of summed moment from 1997 to 2015 for arbitrary 0.5 degree bins of SSEs considered in this study to the total summed moment of earthquakes and SSEs. In each bin that SSEs are pervasive, SSEs constitute the majority of the summed moment. We use a shear modulus of 1.3 GPa (Schumann et al., 2014) and inversion-derived fault parameters to calculate the moment of slow slip events. Earthquake moments are sourced from the NIED F-Net catalog.

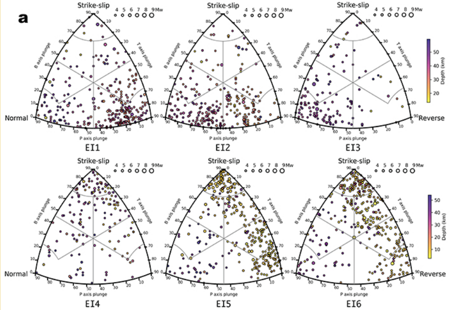

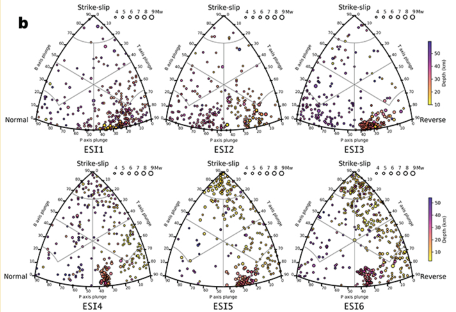

Figure 4 (left). Ternary diagrams of the focal mechanisms comprising (a) groups EI1-EI6, identified in Figure 6c, from the earthquake-only inversion, and (b) groups ESI1-ESI6, identified in Figure 6d, from the earthquake and SSE inversion. Groups that share the same number represent similar spatial areas between the two inversions. SSEs appear as clusters of points. Ternary diagrams generated with FMC (Alvarez-Gomez ,2019) Focal mechanisms are denoted by black-outlined circles filled to indicate event depth in km, and sized to indicate the moment magnitude of the event.

RESULTS

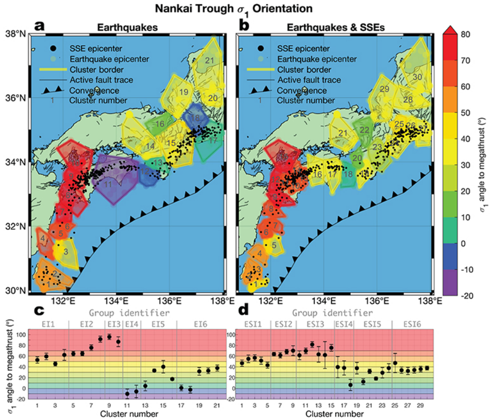

Figure 5. Results of stress inversions for two cases of inputs. (a) Spatial distribution of the orientation of σ_1 to the megathrust for the case of earthquakes only. Clusters numbers are indicated by grey integers. Angles of σ_1 to the megathrust above 80 degrees saturate the colorbar for clusters 8 and 9. (b) Same as (a), but for earthquakes and SSE. (c) σ_1 to the megathrust vs. cluster number for earthquake clusters. Error bars indicate the 95% confidence interval. Groups of clusters that span similar spatial areas between the two inversions are denoted by vertical grey lines and the corresponding group identifier. (d) Same as (c), but for earthquakes and SSE.

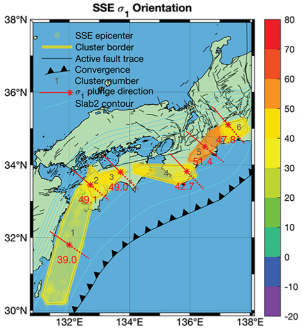

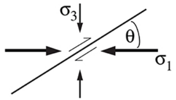

Figure 6 (left). The spatial distribution of the orientation of σ1 to the megathrust for the case of SSEs only. Clusters numbers are indicated by grey integers. The orientation of σ1 is denoted by red lines. Red numbers denote the plunge of σ1 relative to the megathrust, which is also indicated by the colorbar. We use the convention of σ1 being the most compressive principal stress. 10 km to 100 km megathrust depth contours from Hayes et al. (2018) are shown as cyan lines.

IMPLICATIONS FOR FAULT MECHANICS

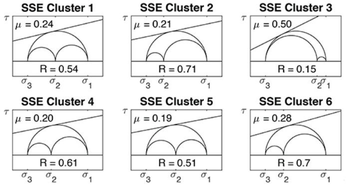

Figure 7 (right). Mohr-Coulomb failure conditions for the SSE clusters shown in Figure 6 determined by iterative stress inversions with a fault instability constraint. R is the shape ratio (Gephart and Forsyth, 1984):

$$R = \frac{\sigma_1 - \sigma_2}{\sigma_1 - \sigma_3}$$

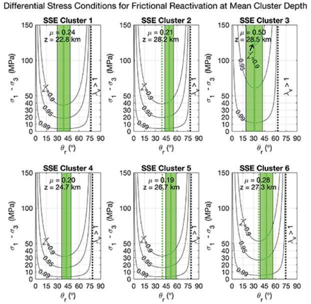

Figure 8 (left). Reactivation plot of differential stress vs. angle of σ_1 to the megathrust for the estimated coefficient of friction and mean cluster depth of each SSE cluster (Figure 6) for different values of the pore fluid factor, λ_v, where $\lambda_v = P_f/\sigma_3$. We assume a pore fluid factor of 0.99 to calculate the hypothetical differential stress of each SSE cluster, shown in Figure 9 below.

$$\sigma_1 - \sigma_3 = \mu_s\left(\frac{\tan\theta_r + \cot\theta_r}{1 - \mu_s \tan\theta_r}\right)\rho g z(1 - \lambda_v)$$

Figure 9 (right). Same as figure 7, but with estimated values of σ_1-σ_3 and σ_1-σ_2 from the angle of σ_1 to the megathrust, the coefficient of friction, and an assumed pore fluid factor of 0.99 at the mean depth of events within each cluster. Recent studies (Warren-Smith, 2019) have shown a temporal variation in R through the slow slip cycle that has been interpreted as fluid pressure cycling. We aim to better understand the temporal evolution of R and λ_v through our future work.

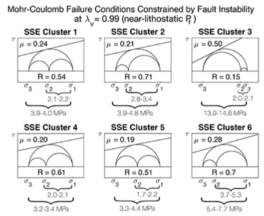

CONCLUSIONS

1. Slow fault slip can be used to constrain the regional stress field.
2. Slow slip events in the Nankai Trough release greater summed seismic moment than earthquakes.
3. The Nankai Trough stress field is well-oriented for the observed tectonic setting.
4. Estimates of the coefficient of friction for SSEs, independent of Pf, suggest the presence of weak materials in the provenance of SSEs.